NANO LETTERS

Letter

pubs.acs.org/NanoLett

Photon Reabsorption Masks Intrinsic Bimolecular Charge-Carrier Recombination in $CH_3NH_3PbI_3$ Perovskite

Timothy W. Crothers,[†] Rebecca L. Milot,[†] Jay B. Patel,[†] Elizabeth S. Parrott,[†] Johannes Schlipf,[‡] Peter Müller-Buschbaum,[‡] Michael B. Johnston,[†] and Laura M. Herz*[,†]

[†]Department of Physics, University of Oxford, Clarendon Laboratory, Parks Road, Oxford OX1 3PU, United Kingdom

[‡]Lehrstuhl für Funktionelle Materialien, Physik-Department, Technische Universität München, James-Franck-Strasse 1, 85748 Garching, Germany

Supporting Information

ABSTRACT: An understanding of charge-carrier recombination processes is essential for the development of hybrid metal halide perovskites for photovoltaic applications. We show that typical measurements of the radiative bimolecular recombination constant in $CH_3NH_3PbI_3$ are strongly affected by photon reabsorption that masks a much larger intrinsic bimolecular recombination rate constant. By investigating a set of films whose thickness varies between 50 and 533 nm, we find that the bimolecular charge recombination rate appears to slow by an order of magnitude as the film thickness increases. However, by using a dynamical model that accounts for photon reabsorption and charge-carrier diffusion we determine that a single intrinsic bimolecular recombination coefficient of value 6.8×10^{-10} cm^3s^{-1} is common to all samples irrespective of film thickness. Hence, we postulate that the wide range of literature values reported for such coefficients is partly to blame on differences in photon out-coupling between samples with crystal grains or mesoporous scaffolds of different sizes influencing light scattering, whereas thinner films or index-matched surrounding layers can reduce the possibility for photon reabsorption. We discuss the critical role of photon confinement on free charge-carrier retention in thin photovoltaic layers and highlight an approach to assess the success of such schemes from transient spectroscopic measurement.

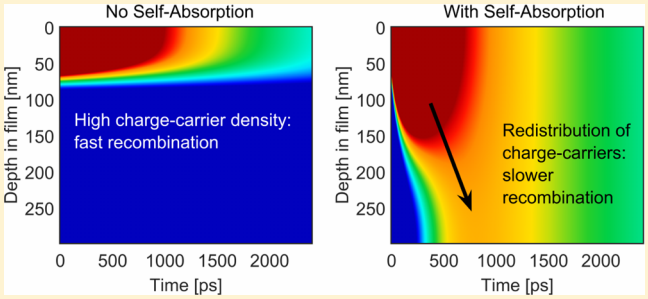

KEYWORDS: *Self-absorption, photovoltaics, THz spectroscopy, charge-carrier recombination*

Within the past few years, the performance of solar cells based on hybrid metal halide perovskites has excelled among other emerging photovoltaic technologies,[1−3] with photoconversion efficiencies (PCEs) now on parity with CdTe and multicrystalline silicon.[4] However, what sets hybrid perovskites apart from typical inorganic semiconductors is that they allow high efficiency to be achieved in conjunction with low processing and material costs.[5] In parallel with the rise in perovskite solar cell performance, research has focused on unravelling the basic physics underlying this success. Studies focusing on the prototypical methylammonium (CH_3NH_3) lead triiodide ($MAPbI_3$) perovskite have uncovered favorable properties typical of traditional inorganic semiconductors, such as a high charge-carrier mobility,[6,7] low exciton binding energy,[8] and the presence of free (uncorrelated) electrons and holes at room temperature.[9,10]

One issue at the center of current debate is the extent to which charge-carrier mobilities and recombination mechanisms result from intrinsic (fundamental) properties of the perovskite or rather from extrinsic factors such as material processing and morphology.[7] In the regime of low charge-carrier density, recombination is mediated by traps and defects[11,12] leading to nonradiative losses that can be reduced by improved material processing.[13−15] Suppression of such extrinsic charge-carrier recombination channels was found to yield favorable monomolecular (trap-mediated) charge-carrier lifetimes in excess of microseconds.[16,17] These improvements have brought into sharp focus the mechanism governing the radiative bimolecular recombination of free electrons and holes, which will begin to dominate at low charge-carrier densities once most traps have been eliminated.[18]

As a first approximation, one would assume the bimolecular recombination between free electrons and holes to be an intrinsic process that is associated with the bandstructure properties of the semiconductor. For classical inorganic semiconductors, bimolecular free-charge recombination is generally viewed as the inverse process of light absorption,[19,20] a relationship that holds across many group IV and III−V semiconductors, such as GaAs.[21] However, adopting such an "intrinsic" view of radiative bimolecular recombination to the case of hybrid perovskites appears to contradict the phenomenally wide range of bimolecular recombination rate

Received: July 5, 2017
Published: August 9, 2017

DOI: 10.1021/acs.nanolett.7b02834
Nano Lett. 2017, 17, 5782−5789

constants that has been reported for any given hybrid perovskite. For example, our literature survey[6,9,10,22−27] reveals that values determined from transient spectroscopy vary by more than an order of magnitude for the most commonly examined $MAPbI_3$ perovskite ($0.6–23 \times 10^{-10}$ cm^3 s^{-1}). Such a widespread suggests at first sight a dependence on extrinsic parameters, such as material morphology. However, this presumption would be at odds with findings that highlight the similarity of the absorption onset of $MAPbI_3$ with that of GaAs,[28] which in analogy with GaAs would result in similarly well-defined intrinsic bimolecular recombination in $MAPbI_3$.

In the current study, we resolve this controversy by showing that the apparent bimolecular recombination rate constant $k_2^{apparent}$ in $MAPbI_3$, as perceived in transient spectroscopy, is strongly modified by photon reabsorption, which masks a much larger intrinsic value of $k_2^{intrinsic}$. As we explain below, such self-absorption of emitted photons can be moderated by external factors such as film thickness, light scattering, or the presence of an interfacing material of different refractive index, which can easily account for the huge spread in apparent values reported.

Self-absorption, or "photon recycling", refers to the process whereby photons generated by radiative recombination of electrons with holes are partially reabsorbed by the emitting material instead of escaping, reducing the apparent rate of radiative recombination. Self-absorption is a familiar process in gases, where spectral lines are broadened by photon reabsorption as the light travels through the emitting medium.[29] In addition, photon reabsorption features prominently in inorganic semiconductors such as GaAs[30,31] because of their strong band-edge absorption and weak Stokes shifts of the emission. In these semiconductors, the high probability of photon reabsorption manifests itself by apparent slow charge-carrier decay rates, as carriers can radiatively recombine and be "recycled" several times before they finally return to the ground state.[32,33] For hybrid metal halide perovskites such as $MAPbI_3$, photon reabsorption has also recently been reported with indications that it may support long-range charge-carrier transport,[34] increase the photoluminescence lifetime,[35] and raise open-circuit voltages[36] or short-circuit currents[37] in perovskite solar cells.

In this Letter, we directly demonstrate that self-absorption of emitted photons can result in a large spread in the apparent value of k_2 in $MAPbI_3$ with film thickness, as perceived in transient spectroscopic experiments. We record the photoexcited charge-carrier population as a function of time using optical-pump THz-probe (OPTP) spectroscopy for a set of evaporated $MAPbI_3$ films whose morphology exhibits no systematic variation with film thickness. We find that the apparent bimolecular recombination rate constant $k_2^{apparent}$ decreases exponentially with increasing film thickness d, from $k_2^{apparent} = 1.4 \times 10^{-10}$ cm^3 s^{-1} for $d = 50$ nm to $k_2^{apparent} = 0.2 \times 10^{-10}$ cm^3 s^{-1} for $d = 533$ nm, indicative of self-absorption that is mediated by Beer's law. However, by use of a model that properly accounts for photon reabsorption and charge-carrier diffusion, we are able to reveal that all films share a single value of the intrinsic bimolecular recombination rate constant, $k_2^{intrinsic} = (6.8 \pm 1.4) \times 10^{-10}$ $cm^3 s^{-1}$, which is remarkably similar to the value for GaAs.[21] We use the model to show how changes in thin-film architecture can strongly affect photon out-coupling through variation in perovskite layer thickness or refractive index of the surroundings, which modifies the apparent rate of bimolecular recombination, thus providing an explanation for the wide spread in literature reports.

Dual-source vapor deposition[38] was used as an ideal technique to produce a set of highly uniform $MAPbI_3$ films of different thickness (50−533 nm) on z-cut quartz substrates. The thickness of the perovskite layers was accurately determined by two different methods that yielded good agreement, that is, through use of a surface profilometer (DekTak) and by optical modeling of reflection and transmission spectra with a transfer matrix model (further detailed in Section 3 in Supporting Information (SI)).

To rule out the influence of potential morphological changes, we first verified that these films exhibit no systematic trends with film thickness for either structural or optical properties or charge-carrier mobilities. Both scanning electron microscopy (SEM) and grazing incidence wide-angle X-ray scattering (GIWAXS) were used to examine the structural properties of these films.[39] SEM images (Figure S1 in SI) demonstrate that all samples have a highly uniform thickness and similar surface morphology across the series with the perovskite layers being composed of a dense network of small grains with ∼100 nm diameter. GIWAXS data (Figure S2 in SI) show a slight variation in the degree of crystal orientation between individual samples that is, however, uncorrelated with film thickness. Together these results show that our samples share similar surface and bulk morphologies across the full film thickness range.

In addition to such structural characterization, we examined the thin-film optical reflection and transmission as well as photoluminescence (PL) spectra of all films. Reflection and transmission spectra were recorded using Fourier transform infrared (FTIR) spectroscopy and analyzed using a transfer matrix model that yields the refractive index and absorption coefficient of the perovskite layers as a function of wavelength (described in Section 3 of the SI). Across our set of samples, we found very similar absorption coefficients with no evident dependence on the film thickness. Steady state PL spectra (Figure S3 in SI) exhibited a slight red-shift in the PL center wavelength from 762 to 766 nm as film thickness increased. However, after the spectra were corrected for photon self-absorption (see Section 6.2 in SI) this red-shift was eliminated, and the corrected PL spectra displayed no trend with thickness.

To probe further for morphological variations, we determined the charge-carrier mobility at terahertz (THz) frequencies across the film series using optical pump THz probe (OPTP) spectroscopy.[40−42] Here, samples were photoexcited by an optical pump pulse at 400 nm wavelength, and the initially recorded photoconductivity was extracted from the change in transmitted THz field amplitude $\Delta T/T$.[41,43] With knowledge of the absorbed photon density per pulse and the assumption of unit photon-to-charge branching ratio, the value of the charge-carrier mobility can then be determined (see SI Section 4.2). Figure 1d shows an average charge-carrier mobility value of (11 ± 2) cm^2 V^{-1} s^{-1} across the series with no apparent correlation with film thickness. The value is commensurate with the relatively small grain size (∼100 nm) typically encountered in these dual-source evaporated $MAPbI_3$ films.[38]

Overall, our analysis of structural, optical, photoluminescence, and charge-carrier mobility data comprehensively demonstrate that these samples exhibit no morphological trends with film thickness. In the following, we are therefore able to focus solely on the effect of film thickness on the apparent charge-carrier dynamics, as mediated by the underlying influence of photon reabsorption.

DOI: 10.1021/acs.nanolett.7b02834
Nano Lett. 2017, 17, 5782−5789

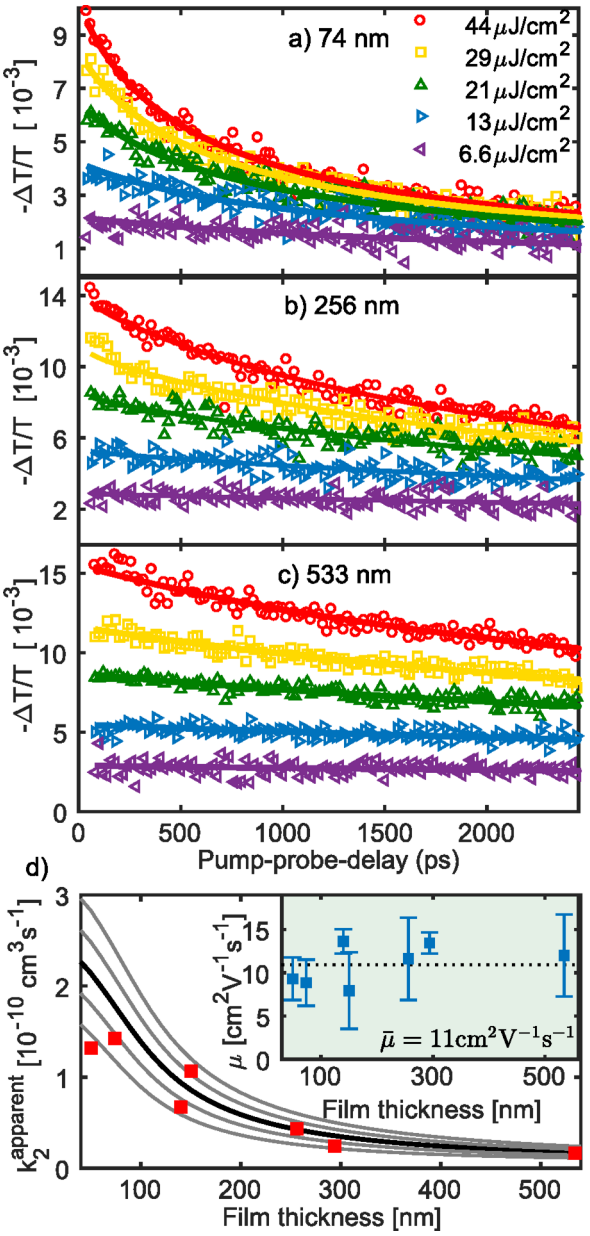

Figure 1. Photoinduced THz conductivity transients for thin films of dual-source vapor deposited $MAPbI_3$ with thicknesses of (a) 74 nm, (b) 256 nm, and (c) 533 nm, following excitation at a wavelength of 400 nm with a range of pulse fluences. Solid lines show global fits to each set, based on the Standard Model described in the text and SI. (d) Variation in $k_2^{apparent}$ (red squares) with film thickness, extracted from fits shown in (a–c). The lines show the modeled dependence of $k_2^{apparent}$ on film thickness predicted by the Self-Absorption Model, which accounts for photon reabsorption and charge-carrier diffusion. The black line shows the best fits based on a film-thickness independent, $k_2^{intrinsic} = 6.8 \times 10^{-10}$ cm^3 s^{-1} with the surrounding grey lines showing the first ($\pm 1.4 \times 10^{-10}$ cm^3 s^{-1}) and second ($\pm 2.8 \times 10^{-10}$ cm^3 s^{-1}) standard deviations. The inset displays the values of the charge-carrier mobility against film thickness, as extracted from OPTP measurements.

To assess the dynamics of the charge-carrier population we recorded photoconductivity transients using OPTP following excitation with 400 nm laser pulses over a range of fluences. Figure 1 shows example photoconductivity transients for three film thicknesses with curves for the full range of samples provided in SI (Figure S10). At the lowest excitation fluence, the decay of the charge-carrier population flattens over the 2.5 ns time window, indicating that monomolecular trap-mediated charge recombination processes occur over much longer time scale, as typical for these materials.[24] With increasing pump-excitation fluence, the transients become increasingly dominated by higher-order processes such as bimolecular electron–hole and Auger recombination. Strikingly, the transients in Figure 1 (and Figure S10) demonstrate a clear trend toward more prominent higher-order recombination processes for thinner samples. Although for a film thickness of 74 nm (Figure 1a) rapid initial decay components are apparent, the photoconductivity decay in the 533 nm sample is relatively slow. For the given observation window and range of fluences, we find bimolecular free-charge-carrier recombination to be the dominant process depleting the charge-carrier population (see Sections 5.4 and 7 of the SI). Therefore, our observations suggest a surprising trend of increasing apparent bimolecular recombination with decreasing film thickness.

To provide a more quantitative assessment of the changes in apparent bimolecular recombination with film thickness, we initially proceed by modeling the charge-carrier density n with a widely used[6,9,44,45] rate equation

$$\frac{dn}{dt} = G - k_3 n^3 - k_2^{apparent} n^2 - k_1 n \quad (1)$$

Here, G is the charge-carrier generation rate; k_1 is the trap-related (nonradiative Shockley-Read-Hall[46]) monomolecular charge-recombination rate; $k_2^{apparent}$ is the radiative bimolecular recombination rate constant of free electrons and holes, as apparent from these transients; and k_3 is the rate constant describing nonradiative Auger recombination between electrons and holes that is mediated by a third charge-carrier.[18] Because of the widespread use of this rate equation to model such transients, we refer to it in the following as the "Standard Model".

Accurate application of this Standard Model to the photoconductivity transients still requires the spatial charge-carrier distribution to be taken into account, as described in full detail in SI (Section 5.2). A correct evaluation is particularly important because higher-order recombination rates are very sensitive to the charge-carrier density n (see eq 1). As the pump pulse travels through the film, its intensity decays exponentially according to Beer's law, which generates a corresponding exponentially decreasing density of charge-carriers through the perovskite film (shown in Figure S9 in SI). To account for this spatial variation along the depth profile we model the perovskite film as a series of slices parallel to the substrate,[47] each of which has a different initial value of n that evolves independently according to eq 1. We then sum over the contributions from all slices to obtain the overall decay of the charge-carrier population, the result of which is fitted globally to each set of experimental photoconductivity transients obtained for the given range of excitation fluences. We may neglect variations in charge-carrier distribution across the lateral dimension of the film because the full width at half-maximum of the pump pulse is much larger (3.9 mm) than that of the THz probe pulse (1.4 mm).

Figure 1d shows that the apparent value $k_2^{apparent}$ of the bimolecular recombination rate constant decreases by roughly 1 order of magnitude with increasing film thickness from 1.4×10^{-10} cm^3 s^{-1} for d = 50 nm to 0.2×10^{-10} cm^3 s^{-1} for d = 533 nm. This variation cannot be caused by differences in material

DOI: 10.1021/acs.nanolett.7b02834
Nano Lett. 2017, 17, 5782–5789

quality or morphology as our measurements discussed above found that there were no correlations between these parameters and film thickness. Therefore, the observed trends in $k_2^{apparent}$ with film thickness suggest that eq 1 does not fully capture the charge-carrier dynamics in these samples. An insight into the problem can be gained by noting that $k_2^{apparent}$ decreases roughly exponentially with film thickness, on a similar length scale to the absorption length of the PL (vide infra). This observation indicates that self-absorption of photons following radiative bimolecular recombination may be responsible for the trend in $k_2^{apparent}$ with film thickness.

To account for such effects, we developed a new model that more accurately describes the charge-carrier dynamics in these films and which incorporates both charge-carrier diffusion and PL self-absorption. This "Self-Absorption Model" follows the treatment of PL self-absorption as successfully implemented for GaAs[32,48] and also includes a diffusion term to account for the effect of charge-carrier motion on leveling the charge-carrier distribution along the film depth profile. Incorporating these two processes, the rate equation governing the density n of free charge-carriers now becomes

$$\frac{\partial n}{\partial t} = D\frac{\partial^2 n}{\partial z^2} + G - k_3 n^3 - k_2 n^2 - k_1 n \quad (2)$$

Here, z is the position in the direction normal to the substrate surface (film depth), and the diffusion coefficient D is set by using the charge-carrier mobility of each sample (shown in Figure 1d). G is again the charge-carrier generation rate, but importantly it now includes not only charge-carrier creation by the initial laser pulse (at zero time) but also charge generation via the reabsorption of photons produced by radiative bimolecular charge-carrier recombination. Photon reabsorption in the perovskite is accounted for by using explicit ray tracing[32] which tracks the propagation of each emitted photon and accounts for possible absorption by the perovskite and reflections at the film boundaries to determine if and where photons are reabsorbed in the film. Full details of the Self-Absorption Model are provided in Section 5.3 of the SI.

Fits based on the Self-Absorption Model to the photoconductivity transients displayed in Figure S10 in SI again yield a value of the bimolecular recombination constant k_2 for each film thickness. However, we now discover that there is no longer any systematic variation with film thickness (see Figure S10) but rather we find a single value of $k_2^{intrinsic} = (6.8 \pm 1.4) \times 10^{-10}$ cm^3 s^{-1} common to all samples. Our Self-Absorption Model therefore reveals that once photon reabsorption is accounted for, these $MAPbI_3$ films display an intrinsic mechanism of bimolecular charge-carrier recombination that is characterized by a single rate constant despite the apparent changes in the shape of the photoconductivity transients. We note that the absolute value of $k_2^{intrinsic}$ we extract for $MAPbI_3$ is remarkably close to that for GaAs (7.2×10^{-10} cm^3 s^{-1}).[21] Given that the absorption onsets of $MAPbI_3$ and GaAs have also been found to be very similar,[28] our finding suggests that bimolecular free-charge recombination may be directly related to the inverse process of light absorption[19,20] in $MAPbI_3$. These phenomena are analogous to what has been observed in inorganic semiconductors such as GaAs[31] and InP[49] for which photon reabsorption has been found to result in a similar reduction of apparent bimolecular recombination with respect to the intrinsic expectation.

We further illustrate how self-absorption masks the intrinsic bimolecular recombination dynamics by showing in Figure 2

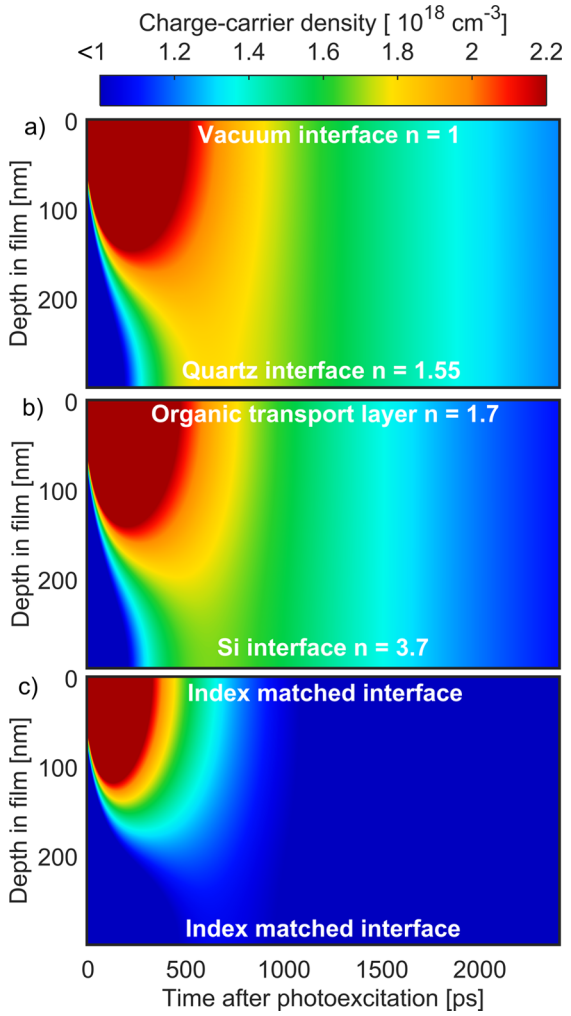

Figure 2. Color plots showing the charge-carrier density evolution with time after excitation and along the film depth profile, as simulated with the Self-Absorption Model that accounts for charge-carrier recombination, diffusion, and photon reabsorption. Simulations are shown over a 2.5 ns time window for (a) an $MAPbI_3$ film on a z-cut quartz disk in vacuum (spectroscopic configuration), (b) a film between an organic hole-transporting layer and monolithic silicon (tandem configuration), and (c) a film between two layers that are index-matched to $MAPbI_3$ (refractive index $n = 2.5$). The model uses the fitted value of $k_2^{intrinsic} = 6.8 \times 10^{-10}$ cm^3 s^{-1} and $k_3 = 1.0 \times 10^{-29}$ cm^6 s^{-1} and assumes a pump excitation fluence of 45 μJ cm^{-2}.

the charge-carrier density decay as a function of depth in the film and time after photoexcitation, as determined by our Self-Absorption Model. Figure 2a examines the case that applies to our transient photoconductivity study, that is, a $MAPbI_3$ film in a "spectroscopic" configuration on a quartz disk and under vacuum. The color plot indicates that initially after photoexcitation, charge-carriers are mostly concentrated at the front of the film, which directly results from the short absorption length of only 25 nm at the excitation wavelength of 400 nm (see Figure S6 in SI). Over time, charge-carriers rapidly spread through the film, until after ~1 ns a flat charge-carrier density profile is present across the full depth profile. This redistribution is driven jointly by diffusion and self-absorption and lowers the peak charge-carrier density, thereby reducing the

DOI: 10.1021/acs.nanolett.7b02834
Nano Lett. 2017, 17, 5782−5789

efficiency of higher-order recombination processes such as bimolecular and Auger recombination.[6] As a result, the charge-carrier population experiences a fast initial decay rate governed by the initially uneven charge-carrier distribution, which is then substantially lowered when the population spreads out. Self-absorption and charge diffusion therefore lead to an apparent lowering of the bimolecular recombination rate constant k_2^{apparent} that masks a much higher intrinsic value $k_2^{\text{intrinsic}}$.

On the basis of these arguments, the apparent thickness dependence of the photoconductivity transients can therefore be explained by the propensity of charge carriers to spread out further in thicker films, which lowers peak charge-carrier density and slows bimolecular recombination. Our Self-Absorption Model shows that indeed, even for the thickest sample examined in our study, photon reabsorption will occur over a sufficient length scale to result in an even spread of charge-carriers through the depth of the film (see Figure S19 in SI). To illustrate this further, we fit the solution to eq 1 within the Standard Model to modeled photoconductivity transients obtained from our Self-Absorption Model, in order to obtain the apparent value of k_2^{apparent} as a function of film thickness (see Section 7 of SI). The resulting dependence is shown as lines in Figure 1d for different values of $k_2^{\text{intrinsic}}$, showing good agreement with the values of k_2^{apparent} extracted by fits of the Standard Model to the experimental transients (red squares). Hence the model incorporating photon reabsorption and charge-carrier diffusion can fully explain the apparent changes in the shape of the transients with film thickness.

The influence of photon reabsorption on the apparent bimolecular recombination rate raises the question of how such processes will be affected by out-coupling of photons from the film. Because hybrid perovskites exhibit a relatively large refractive index at optical frequencies (e.g., n_{per} = 2.5 for $MAPbI_3$, see Figure S6b in SI), strong dependencies can be expected on the refractive index of the surrounding layers. To illustrate such effects, Figure 2 shows the time-dependent charge-carrier density distributions also for the cases of (b) an $MAPbI_3$ film surrounded by infinitely thick layers of silicon on one side and a typical organic transport layer on the other, such as may be encountered in a perovskite-silicon tandem cell, and (c) an $MAPbI_3$ film index-matched to its surroundings. We note that our modeling of photon out-coupling does not include thin-film interference effects, which would modify the effect somewhat,[36] but would give a specific dependence on overall layer architecture that we neglect at this point to allow for a better qualitative comparison.

Figure 2 hence illustrates the evolution of the charge-carrier distribution inside a $MAPbI_3$ film with (a) high, (b) intermediate, and (c) no photon confinement. The stark changes between the three scenarios are directly attributable to the large absorption length of the emitted PL in $MAPbI_3$, which is a multiple of the typical film thickness. As a result, the extent of photon reabsorption is mostly determined by the strength of the photon confinement within the perovskite layer, which is influenced by the refractive index of the surrounding layers through the modification of total internal reflection. Figure 2c illustrates that for fully index-matched surroundings, when most photons leave the film without being reabsorbed, the charge-carrier density decays swiftly and with only minor redistribution caused by charge-carrier diffusion, which is a weak effect over this time interval (see also Section 9.2 in SI). As a result, the apparent bimolecular recombination rate increases, meaning that k_2^{apparent} becomes closer to the value of $k_2^{\text{intrinsic}}$.

Our evaluation of photon out-coupling effects has important consequences for the analysis of spectroscopic transients recorded for these materials. First, we show that the closer the apparently observed bimolecular recombination rate constants are to the intrinsic values, the more photons are allowed to leave the film. This can be facilitated e.g. through index-matching with the surrounding layers, or light scattering effects. Second, we note that the dependence of photon out-coupling on the refractive index of the surrounding layers means that the addition of a charge-extraction layer on top of a perovskite film will modify the shape of the observed transients even in the absence of charge-transfer across that interface. Therefore, such transients require careful analysis before quantitative deductions on the charge-transfer efficiencies can be made.

To assess further the effects of photon out-coupling we proceed by calculating the correction factor Φ_2 that is required in order to obtain intrinsic values $k_2^{\text{intrinsic}}$ from the apparent values k_2^{apparent} typically deduced from data by use of the Standard Model, with

$$\Phi_2 = \frac{k_2^{\text{apparent}}}{k_2^{\text{intrinsic}}} \tag{3}$$

such that lower values of Φ_2 denote slower charge-carrier recombination in a system. To determine Φ_2, the Self-Absorption Model is used to generate a set of photoconductivity transients based on the intrinsic value $k_2^{\text{intrinsic}}$, which are then globally fitted using the Standard Model to determine the apparent value k_2^{apparent} (see Section S7 in SI). These calculations are conducted for an assumed even charge-carrier distribution through the film. We explore the effect of photon confinement by calculating the correction factor Φ_2 for a 300 nm thick perovskite layer sandwiched between two infinitely thick layers with a range of refractive indices, shown in Figure 3a. When at least one of the interfacial layers has a higher refractive index than the perovskite (2.5), Φ_2 is always greater than 50%, as there is no total internal reflection to enhance the photon confinement. When both of the surrounding layers are lower in refractive index than the perovskite, Φ_2 decreases sharply as photon confinement is boosted. The wide range of values encountered for Φ_2 show the sensitivity of charge-carrier retention on the type of surroundings the film is embedded in.

Figure 3a clearly highlights the potential downside of incorporating perovskites into indexed-matched surrounds. For example, for the configurations selected in Figure 2 the probability of photon reabsorption falls from 78% for layers on quartz substrates, to 47% in the simplified silicon-tandem configuration, and only 34% for indexed matched interfaces. These scenarios indicate real losses since the apparent value k_2^{apparent} reflects the rate with which charge-carriers are lost from the system, while the value of $k_2^{\text{intrinsic}}$ represents only the intrinsic loss through bimolecular charge-carrier recombination and therefore photon generation inside the material. As pointed out in recent studies,[34−36] such losses become more important as parasitic nonradiative recombination via traps is reduced. In high-quality thin films of $MAPbI_3$, trap-related recombination rates on the order of microseconds are already becoming reality.[16,17,50,51] These advances thus highlight the need for enhanced photon confinement to further reduce charge-carrier losses from the perovskite. Such photon management may for example be achieved through placing light-trapping structures

DOI: 10.1021/acs.nanolett.7b02834
Nano Lett. 2017, 17, 5782−5789

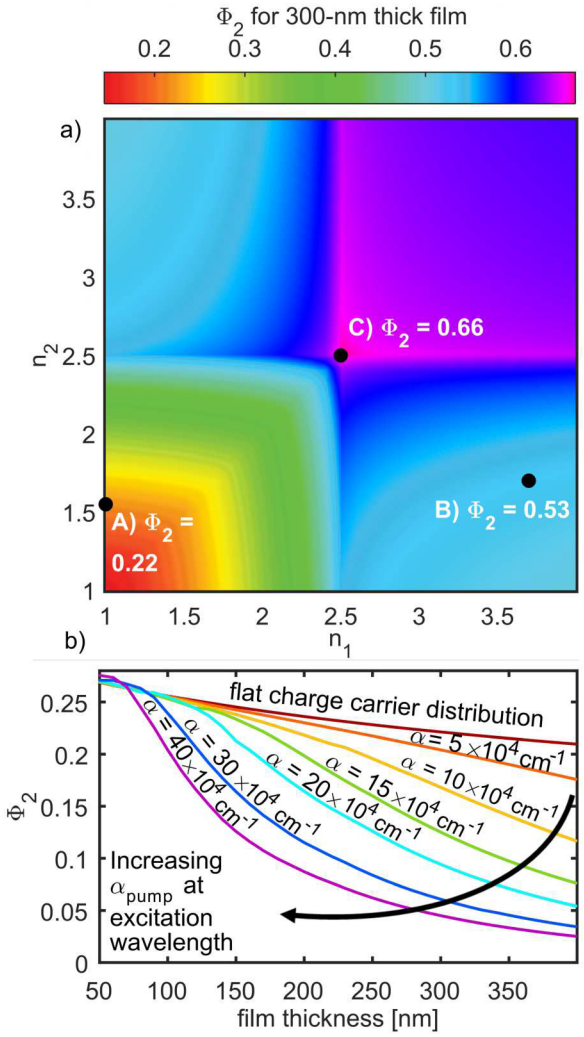

Figure 3. (a) Simulated ratio $\Phi_2 = k_2^{apparent}/k_2^{intrinsic}$ of the apparent to the intrinsic bimolecular recombination rate, with $k_2^{intrinsic} = 6.8 \times 10^{-10}$ cm^3 s^{-1}. Φ_2 was evaluated using the Self-Absorption Model described in the text for an even initial distribution of charge-carriers along the film depth profile. The model assumes a 300 nm thick layer of perovskite (n = 2.5), sandwiched between two infinitely thick interfacing layers. The points A−C represent the modeled examples in Figure 2a−c. (b) Simulated variation of Φ_2 as a function of thickness shown for different values of the absorption coefficient experienced at a given excitation (pump) wavelength by a $MAPbI_3$ perovskite film on a quartz substrate. Higher absorption coefficients lead to a less even initial charge-carrier distribution through the film depth profile.

around solar cells[52] or texturing of the cell surface.[35,53] Ultimately the correct management of radiative losses determines the maximum efficiency of a solar cell,[54] and as light management is already a limiting factor in perovskite devices,[55] further consideration of photon management will become an important element in device design.

Finally, we use our findings to highlight some of the potential causes for the wide spread in apparent values of k_2 reported in the literature for a range of different hybrid metal perovskites. We first focus on variations in material morphology that may affect light reabsorption through scattering and subsequently comment on the effect of compositional changes such as halide substitution.

A number of independent studies have reported that bimolecular recombination constants appeared to be higher for lead iodide perovskite films with smaller grain size.[6,25,56] Such effects are surprising at first sight. Extrinsic trap-mediated recombination may well be affected by grain size because of a potential propensity of traps to accumulate at grain boundaries.[57] However, the bimolecular recombination between free electrons and holes is normally governed by the band-edge density of states that is intrinsic to the semiconductor, which should be largely unaffected by grain size given that $MAPbI_3$ exhibits an energetically sharp absorption onset.[28] To explain the dependence of the apparent bimolecular recombination rate constant on grain size we note that in these films, the lateral extent of the grains is typically on a length scale comparable to the PL wavelength. Hence changes in grain size will strongly affect the extent of Rayleigh scattering from crystal defects in both the bulk and surface of the material, which is known to limit the free path length of PL.[36,53] A scattering event can alter the direction of a traveling photons, allowing photons previously confined by total internal reflection to escape.[36] As we show above, the lowered photon confinement will result in an increase in the apparent bimolecular recombination rate constant $k_2^{apparent}$ that is perceived in transient spectroscopy. These considerations can thus not only explain the dependence of $k_2^{apparent}$ on grain size but also the faster bimolecular recombination reported for hybrid perovskites infused into mesoporous oxide scaffolds[6,56,58] which scatter strongly, leading to reduced photon retention. Although a full consideration of scattering mechanism involved[53] is beyond this study, we propose that the wide range in bimolecular recombination rates reported for $MAPbI_3$ in the literature may largely derive from an indirect impact of the film morphology and thickness, which mask the underlying existence of a single, intrinsic value $k_2^{intrinsic}$ of the bimolecular rate constant.

In addition, we consider the impact of halide substitution on the apparent bimolecular rate constant perceived in transient spectroscopy. Several literature studies have reported bimolecular charge-carrier recombination dynamics to be more rapid in bromide lead perovskites compared to the equivalent iodide lead perovskites.[44,59,60] Rehman et al. found $k_2^{apparent}$ to increase steadily by about 1 order of magnitude with increasing bromide fraction x in thin films of $FAPb(Br_xI_{1-x})_3$[44] and $Cs_yFA_{1-y}Pb(Br_xI_{1-x})_3$[60] which they attributed to gradual changes in the bandstructure. We note here that the associated increase in bandgap with increasing bromide content will lead to a decrease in the density of the absorbing states at the fixed laser excitation typically employed by these experiments (the excitation in effect moves closer in energy to the gap). As a result, the absorption length for photons inside the material increases, giving rise to a more even initial distribution of charge-carriers across the depth profile which may, in turn, affect the subsequent charge-carrier dynamics.

To exemplify such effects, Figure 3b shows how the ratio Φ_2 between the apparent bimolecular recombination rate constant, $k_2^{apparent}$, and the intrinsic value $k_2^{intrinsic}$ changes as a function of film thickness, for a range of different absorption coefficient values α experienced at the excitation wavelength. Since $k_2^{intrinsic}$ is independent of film thickness and photon wavelength, these curves in essence chart the change in the apparent rate constant $k_2^{apparent}$ that is perceived in transient spectroscopy following pulsed excitation. These curves show that for high absorption coefficient or short penetration depth (purple curve) at the

DOI: 10.1021/acs.nanolett.7b02834
Nano Lett. 2017, 17, 5782−5789

excitation wavelength, the bimolecular recombination appears to be particularly severely suppressed for large film thickness. This effect results from the rapid redistribution of charge-carriers induced by photon reabsorption that flattens the charge-carrier profile soon after excitation (see Figure 2a). As a consequence, fits to the transients using the Standard Model return a particularly low value of the bimolecular recombination constant with respect to the intrinsic value. We note that even for an initially flat (even) charge-carrier distribution (red curve) photon reabsorption will still reduce the apparent rate constant k_2^{apparent} below the intrinsic value, because reabsorbed photons regenerate charge-carriers at later stages, thus maintaining a high charge-carrier density over longer times. However, the factor Φ_2 is particularly low for large film thicknesses and uneven initial charge-carrier density profiles, for which photon reabsorption has the strongest redistributive influence. With relevance to the influence of halide substitution, one has to consider that for the $MAPbX_3$ system the absorption coefficient for a given excitation wavelength of 400 nm falls by a factor 4 when X is changed from I to Br.[61] Figure 3b shows that this change alone would introduce a reduction by a factor 4.2 in k_2^{apparent} as measured following pulsed excitation (see SI for details). Therefore, changes in photon reabsorption with changing bandgap energy are partly to blame for the observed order-of-magnitude difference in k_2^{apparent}, with changes in the band-edge density of states the most likely cause for the remaining trend.

In summary, we have demonstrated that reabsorption of emitted photons masks a much higher underlying intrinsic rate of bimolecular recombination of electrons with holes. We find that such self-absorption is particularly prominent in thick films, where it leads to a pronounced reduction in the apparent bimolecular rate constant associated with the charge-carrier density transients. By accounting for photon reabsorption and charge-carrier diffusion, we were able to show that, irrespective of thickness, all films share a common intrinsic value of the bimolecular recombination rate constant of $k_2^{\text{intrinsic}} = (6.8 \pm 1.4) \times 10^{-10}$ cm^3 s^{-1}. These results suggest that the wide range of values reported in the literature for $MAPbI_3$ are most likely caused by variations in film thickness and light out-coupling, with the latter resulting, for example, from scattering off crystal grains with different nanoscale sizes, or an underlying mesoscopic metal-oxide structure. Our findings further link the apparent bimolecular recombination constants perceived in transient spectroscopy with the overall charge-carrier retention strategies achieved through photon management. Because k_2^{apparent} in essence captures the real dynamics of the bimolecular charge-carrier density decay, which includes radiative recombination and photon reabsorption effects, it can serve as an indicator of the extent to which the photon retention has been achieved. Hence the success of photon management strategies can be conveniently evaluated in a contactless manner by recording spectroscopic transients for full solar cell device structures and comparing extracted values of k_2^{apparent} against the intrinsic value $k_2^{\text{intrinsic}}$ we have determined here. We show that for typical layer structures surrounding lead halide perovskite in a photovoltaic device, photon retention is clearly suppressed, highlighting the need for additional photon management strategies as these devices approach the Shockley-Queisser limit.

■ ASSOCIATED CONTENT

Supporting Information

The Supporting Information is available free of charge on the ACS Publications website at DOI: 10.1021/acs.nanolett.7b02834.

Material preparation; structural and optical characterization data; description of FTIR transfer matrix model and extraction of complex refractive index; OPTP experimental details; description of ray tracing model for self absorption; quantitative relation between self-absorption and Standard Models of charge carrier dynamics; additional modeling results from Self-Absorption Model (PDF)

■ AUTHOR INFORMATION

Corresponding Author

*E-mail: laura.herz@physics.ox.ac.uk.

ORCID

Elizabeth S. Parrott: 0000-0003-3165-4608
Johannes Schlipf: 0000-0001-8692-6389
Peter Müller-Buschbaum: 0000-0002-9566-6088
Michael B. Johnston: 0000-0002-0301-8033
Laura M. Herz: 0000-0001-9621-334X

Notes

The authors declare no competing financial interest.

■ ACKNOWLEDGMENTS

This work was funded by the U.K.'s Engineering and Physical Sciences Research (EPSRC). J.S. and P.M.-B. acknowledge funding from the Bavarian research network "Solar Technologies Go Hybrid" (SolTech) and from the Excellence Cluster "Nanosystems Initiative Munich" (NIM). J.S. and P.M.-B. thank Wiebke Ohm and Lorenz Bießmann for help with setting up the beamline P03 at DESY.

■ REFERENCES

(1) Lee, M. M.; Teuscher, J.; Miyasaka, T.; Murakami, T. N.; Snaith, H. J. *Science* **2012**, *338*, 643−647.
(2) Liu, M.; Johnston, M. B.; Snaith, H. J. *Nature* **2013**, *501*, 395−398.
(3) Li, X.; Bi, D.; Yi, C.; Decoppet, J.-D.; Luo, J.; Zakeeruddin, S. M.; Hagfeldt, A.; Gratzel, M. *Science* **2016**, *353*, 58−62.
(4) Green, M. A.; Emery, K.; Hishikawa, Y.; Warta, W.; Dunlop, E. D. *Prog. Photovoltaics* **2016**, *24*, 905−913.
(5) Snaith, H. J. *J. Phys. Chem. Lett.* **2013**, *4*, 3623−3630.
(6) Wehrenfennig, C.; Eperon, G. E.; Johnston, M. B.; Snaith, H. J.; Herz, L. M. *Adv. Mater.* **2014**, *26*, 1584−1589.
(7) Herz, L. M. *ACS Energy Letters* **2017**, *2*, 1539−1548.
(8) Galkowski, K.; Mitioglu, A.; Miyata, A.; Plochocka, P.; Portugall, O.; Eperon, G. E.; Wang, J. T. W.; Stergiopoulos, T.; Stranks, S. D.; Snaith, H.; Nicholas, R. J. *Energy Environ. Sci.* **2016**, *9*, 962−970.
(9) Trinh, M. T.; Wu, X.; Niesner, D.; Zhu, X. *J. Mater. Chem. A* **2015**, *3*, 9285−9290.
(10) Yamada, Y.; Nakamura, T.; Endo, M.; Wakamiya, A.; Kanemitsu, Y. *J. Am. Chem. Soc.* **2014**, *136*, 11610−11613.
(11) Draguta, S.; Thakur, S.; Morozov, Y. V.; Wang, Y.; Manser, J. S.; Kamat, P. V.; Kuno, M. *J. Phys. Chem. Lett.* **2016**, *7*, 715−721.
(12) Herz, L. M. *Annu. Rev. Phys. Chem.* **2016**, *67*, 65−89.
(13) Stewart, R. J.; Grieco, C.; Larsen, A. V.; Maier, J. J.; Asbury, J. B. *J. Phys. Chem. Lett.* **2016**, *7*, 1148−1153.
(14) Ham, S.; Choi, Y. J.; Lee, J.-W.; Park, N.-G.; Kim, D. *J. Phys. Chem. C* **2017**, *121*, 3143−3148.

DOI: 10.1021/acs.nanolett.7b02834
Nano Lett. 2017, 17, 5782−5789

(15) Ziang, X.; Shifeng, L.; Laixiang, Q.; Shuping, P.; Wei, W.; Yu, Y.; Li, Y.; Zhijian, C.; Shufeng, W.; Honglin, D.; Minghui, Y.; Qin, G. G. *Opt. Mater. Express* **2015**, *5*, 29−43.
(16) DeQuilettes, D. W.; Koch, S.; Burke, S.; Paranji, R. K.; Shropshire, A. J.; Ziffer, M. E.; Ginger, D. S. *ACS Energy Lett.* **2016**, *1*, 438−444.
(17) Zhumekenov, A. A.; Saidaminov, M. I.; Haque, M. A.; Alarousu, E.; Sarmah, S. P.; Murali, B.; Dursun, I.; Miao, X.-H.; Abdelhady, A. L.; Wu, T.; Mohammed, O. F.; Bakr, O. M. *ACS Energy Lett.* **2016**, *1*, 32−37.
(18) Johnston, M. B.; Herz, L. M. *Acc. Chem. Res.* **2016**, *49*, 146−154.
(19) Bhattacharya, R.; Pal, B.; Bansal, B. *Appl. Phys. Lett.* **2012**, *100*, 222103.
(20) Van Roosbroeck, W.; Shockley, W. *Phys. Rev.* **1954**, *94*, 1558−1560.
(21) Varshni, Y. P. *Phys. Status Solidi B* **1967**, *19*, 459−514.
(22) Milot, R. L.; Eperon, G. E.; Snaith, H. J.; Johnston, M. B.; Herz, L. M. *Adv. Funct. Mater.* **2015**, *25*, 6218−6227.
(23) Manser, J. S.; Kamat, P. V. *Nat. Photonics* **2014**, *8*, 737−743.
(24) Wehrenfennig, C.; Liu, M.; Snaith, H. J.; Johnston, M. B.; Herz, L. M. *Energy Environ. Sci.* **2014**, *7*, 2269−2275.
(25) D'Innocenzo, V.; Kandada, A. R. S.; De Bastiani, M.; Gandini, M.; Petrozza, A. *J. Am. Chem. Soc.* **2014**, *136*, 17730−17733.
(26) Savenije, T. J.; Ponseca, C. S.; Kunneman, L.; Abdellah, M.; Zheng, K.; Tian, Y.; Zhu, Q.; Canton, S. E.; Scheblykin, I. G.; Pullerits, T.; Yartsev, A.; Sundström, V. *J. Phys. Chem. Lett.* **2014**, *5*, 2189−2194.
(27) Guo, Z.; Manser, J. S.; Wan, Y.; Kamat, P. V.; Huang, L. *Nat. Commun.* **2015**, *6*, 7471−7478.
(28) De Wolf, S.; Holovsky, J.; Moon, S. J.; Löper, P.; Niesen, B.; Ledinsky, M.; Haug, F. J.; Yum, J. H.; Ballif, C. *J. Phys. Chem. Lett.* **2014**, *5*, 1035−1039.
(29) Bonner, T. W. *Phys. Rev.* **1932**, *40*, 105−111.
(30) Ettenberg, M.; Kressel, H. *J. Appl. Phys.* **1976**, *47*, 1538−1544.
(31) Asbeck, P. *J. Appl. Phys.* **1977**, *48*, 820−822.
(32) Steiner, M. A.; Geisz, J. F.; García, I.; Friedman, D. J.; Duda, A.; Kurtz, S. R. *J. Appl. Phys.* **2013**, *113*, 123109.
(33) Ahrenkiel, R. K.; Dunlavy, D. J.; Keyes, B.; Vernon, S. M.; Dixon, T. M.; Tobin, S. P.; Miller, K. L.; Hayes, R. E.; Ahrenkie, R. K.; Dunlavy, D. J.; Keyes, B. *Appl. Phys. Lett.* **1989**, *55*, 1088−1090.
(34) Pazos-Outon, L. M.; Szumilo, M.; Lamboll, R.; Richter, J. M.; Crespo-Quesada, M.; Abdi-Jalebi, M.; Beeson, H. J.; Vrucinic, M.; Alsari, M.; Snaith, H. J.; Ehrler, B.; Friend, R. H.; Deschler, F. *Science* **2016**, *351*, 1430−1433.
(35) Richter, J. M.; Abdi-Jalebi, M.; Sadhanala, A.; Tabachnyk, M.; Rivett, J. P.; Pazos-Outón, L. M.; Gödel, K. C.; Price, M.; Deschler, F.; Friend, R. H. *Nat. Commun.* **2016**, *7*, 13941.
(36) Kirchartz, T.; Staub, F.; Rau, U. *ACS Energy Lett.* **2016**, *1*, 731−739.
(37) Saliba, M.; Zhang, W.; Burlakov, V. M.; Stranks, S. D.; Sun, Y.; Ball, J. M.; Johnston, M. B.; Goriely, A.; Wiesner, U.; Snaith, H. J. *Adv. Funct. Mater.* **2015**, *25*, 5038−5046.
(38) Patel, J. B.; Wong-Leung, J.; Van Reenen, S.; Sakai, N.; Wang, J. T. W.; Parrott, E. S.; Liu, M.; Snaith, H. J.; Herz, L. M.; Johnston, M. B. *Adv. Electron. Mater.* **2017**, *3*, 1600470.
(39) Schlipf, J.; Müller-Buschbaum, P. *Adv. Energy Mater.* **2017**, 1700131.
(40) Ulbricht, R.; Hendry, E.; Shan, J.; Heinz, T. F.; Bonn, M. *Rev. Mod. Phys.* **2011**, *83*, 543−586.
(41) Tiwana, P.; Docampo, P.; Johnston, M. B.; Herz, L.; Snaith, H. *Energy Environ. Sci.* **2012**, *5*, 9566−9573.
(42) Docampo, P.; Tiwana, P.; Sakai, N.; Miura, H.; Herz, L.; Murakami, T.; Snaith, H. J. *J. Phys. Chem. C* **2012**, *116*, 22840−22846.
(43) Nienhuys, H.-K.; Sundström, V. *Phys. Rev. B: Condens. Matter Mater. Phys.* **2005**, *71*, 235110.
(44) Rehman, W.; Milot, R. L.; Eperon, G. E.; Wehrenfennig, C.; Boland, J. L.; Snaith, H. J.; Johnston, M. B.; Herz, L. M. *Adv. Mater.* **2015**, *27*, 7938−7944.
(45) Milot, R. L.; Sutton, R. J.; Eperon, G. E.; Haghighirad, A. A.; Hardigree, J. M.; Miranda, L.; Snaith, H. J.; Johnston, M. B.; Herz, L. M. *Nano Lett.* **2016**, *16*, 7001−7007.
(46) Shockley, W.; Read, W. T. *Phys. Rev.* **1952**, *87*, 835−842.
(47) Wehrenfennig, C.; Liu, M.; Snaith, H. J.; Johnston, M. B.; Herz, L. M. *J. Phys. Chem. Lett.* **2014**, *5*, 1300−1306.
(48) Balenzategui, J. L.; Marti, A. *Sol. Energy Mater. Sol. Cells* **2006**, *90*, 1068−1088.
(49) Parrott, J. E. *Sol. Energy Mater. Sol. Cells* **1993**, *30*, 221−231.
(50) Chen, Y.; Yi, H. T.; Wu, X.; Haroldson, R.; Gartstein, Y. N.; Rodionov, Y. I.; Tikhonov, K. S.; Zakhidov, A.; Zhu, X. Y.; Podzorov, V. *Nat. Commun.* **2016**, *7*, 12253.
(51) Khan, M. R.; Wang, X.; Asadpour, R.; Lundstrom, M.; Alam, M. A. 2016, arXiv:1612.06731. Accessed 4/26/2107.
(52) Reuter, H.; Schmitt, H. *Sol. Energy Mater. Sol. Cells* **1994**, *33*, 369−377.
(53) Poruba, a.; Fejfar, A.; Remeš, Z.; Špringer, J.; Vaněček, M.; Kočka, J.; Meier, J.; Torres, P.; Shah, A. *J. Appl. Phys.* **2000**, *88*, 148−160.
(54) Martí, A.; Balenzategui, J. L.; Reyna, R. *J. Appl. Phys.* **1997**, *82*, 4067−4075.
(55) Polman, A.; Knight, M.; Garnett, E. C.; Ehrler, B.; Sinke, W. C. *Science* **2016**, *352*, aad4424−aad4424.
(56) Hutter, E. M.; Eperon, G. E.; Stranks, S. D.; Savenije, T. J. *J. Phys. Chem. Lett.* **2015**, *6*, 3082−3090.
(57) DeQuilettes, D. W.; Vorpahl, S. M.; Stranks, S. D.; Nagaoka, H.; Eperon, G. E.; Ziffer, M. E.; Snaith, H. J.; Ginger, D. S. *Science* **2015**, *348*, 683−686.
(58) De Bastiani, M.; D'Innocenzo, V.; Stranks, S. D.; Snaith, H. J.; Petrozza, A. *APL Mater.* **2014**, *2*, 081509.
(59) Yang, Y.; Yang, M.; Li, Z.; Crisp, R.; Zhu, K.; Beard, M. C. *J. Phys. Chem. Lett.* **2015**, *6*, 4688−4692.
(60) Rehman, W.; McMeekin, D. P.; Patel, J. B.; Milot, R. L.; Johnston, M. B.; Snaith, H. J.; Herz, L. M. *Energy Environ. Sci.* **2017**, *10*, 361−369.
(61) Leguy, A.; Azarhoosh, P.; Alonso, M. I.; Campoy-Quiles, M.; Weber, O. J.; Yao, J.; Bryant, D.; Weller, M. T.; Nelson, J.; Walsh, A.; van Schilfgaarde, M.; Barnes, P. R. F. *Nanoscale* **2016**, *8*, 6317−6327.

DOI: 10.1021/acs.nanolett.7b02834
Nano Lett. 2017, 17, 5782−5789